

11. The sunward libration point is located on a line joining the sun and the earth and is approximately 1.5×10^8 km from the earth. Because of the alignment with the sun, telemetry signals from a spacecraft located in the vicinity of this point will be degraded significantly by solar interference. This problem can be eliminated by placing the spacecraft into a halo orbit around the libration point. As viewed from the earth, such a spacecraft would appear to be in an elongated orbit around the sun. Although halo orbit is inherently unstable, fuel requirements to maintain it are modest.
12. Inquiries should be sent to Dr. J. I. Vette, National Space Science Data Center, NASA/Goddard Space Flight Center, Greenbelt, Maryland 20771.
13. The magnetosphere exhibits a phenomenon of instability called a "magnetic substorm," and these are presently the subject of considerable interest and controversy. See, for example, S. I. Akasofu, *Physics of Magnetospheric Substorms* (Reidel, Dordrecht, 1977); R. L. McPherron, *J. Geophys. Res.* **75**, 5592 (1970); C. T. Russell and R. L. McPherron, *Space Sci. Rev.* **14**, 205 (1973).
14. Magnetospheric plasma is reviewed in L. A. Frank, *Rev. Geophys. Space Phys.* **13**, 974 (1975); magnetospheric magnetic fields are reviewed in C. T. Russell, *Rev. Geophys. Space Phys.* **13**, 952 (1975); V. M. Vasyliunas, in *Solar-Terrestrial Physics*, E. R. Dyer, Ed. (Reidel, Dordrecht, 1972), part 3, p. 192; R. A. Wolf, *Space Sci. Rev.* **17**, 537 (1975); S. I. Akasofu and S. Chapman, *Solar-Terrestrial Physics* (Oxford Univ. Press, London, 1972), p. 197.
15. G. L. Siscoe, in *Solar System Plasma Physics*, C. F. Kennel *et al.*, Eds. (North-Holland, Amsterdam, 1977).
16. An example of the extensive literature on pulsations is R. L. McPherron *et al.*, *Space Sci. Rev.* **13**, 411 (1972).
17. L. A. Frank, K. L. Akerson, R. P. Lepping, *J. Geophys. Res.* **81**, 5859 (1976).
18. S. J. Bame, J. R. Asbridge, W. C. Feldman, P. D. Kearney, *Solar Phys.* **35**, 137 (1974); J. T. Noble *et al.*, *ibid.* **46**, 303 (1976).
19. A. F. Timothy, A. S. Krieger, G. S. Viana, *ibid.* **42**, 135 (1975).
20. R. J. Fitzenreiter, J. Fainberg, R. R. Weber, H. Alvarez, F. T. Haddock, W. H. Potter, *ibid.* in press.
21. R. N. Klebesadel, I. B. Strong, R. A. Olsen, *Astrophys. J. Lett.* **182**, 2 (1973); *ibid.*, p. 85.
22. GEOS is described in *ESA Bulletin No. 9* (European Space Agency, Paris, 1977).
23. This refers to the later members of the IMP series, which were open-ended multifaceted cylinders, spin-stabilized with the spin axis perpendicular to the ecliptic.
24. An international project of this magnitude involves many people and organizations and is built on the previous efforts of many others. It is not possible to acknowledge all participants by name but a glance at Table 2 indicates how many organizations are involved.

Ocean Surface Currents Mapped by Radar

Mobile coastal units can map variable surface currents
in real time to 70 kilometers, using ocean wave scatter.

D. E. Barrick, M. W. Evans, B. L. Weber

Currents within 1 meter of the ocean surface are highly variable, being driven by geostrophic forces and tides, but are strongly influenced by the local surface wind and wave fields. These currents transport floating matter and thus are of great importance in coastal areas, where considerable damage can be done by surface-borne pollutants and oil. In the case of the large oil spill by the tanker *Argo Merchant* off New England in December 1976, for example, catastrophic environmental damage was averted because strong offshore winds counteracted the normal surface-current drift toward shore. In a positive vein, the upper portion of the sea carries the zooplankton and phytoplankton, which are the dominant components at the bottom of the food chain and are responsible for production of most of the world's oxygen. Many types of fish eggs are borne by surface currents, which are therefore of concern to the fisheries industry. The transport of water with anomalous tem-

perature differences is now believed to be responsible for unusual weather patterns affecting entire continents.

Near-surface current patterns, and how they respond locally to the relevant prevailing forces, are a subject that is largely unknown. Yet the subject is a crucial ingredient for the effective management of operations in coastal waters, and an increasingly important input for global resource monitoring and weather predictions.

Current Measurements

In conventional methods of measuring currents moored meters are used; the most recent types are referred to as vector-averaging current meters and the Aanderaa meter (1). These devices must be moored at depths exceeding 10 m, and thus provide little indication of the current at the surface, which is often different. Furthermore, data must be either recorded aboard the buoy (to be picked up later for analysis) or telemetered to shore; the instrumentation for the latter often restricts the operating range from

the receiver to tens of kilometers. Surface currents have been measured by tracking floating objects. Qualitative estimates can be obtained by photographing the dispersal of dye packages from an aircraft, or by analyzing satellite infrared and optical imagery of suspended sediment (to a coarser area scale) (2). Quantitative measurements are made by photographically recording the positions of time-released floats dropped from the air, as described by Richardson *et al.* (3), or by tracking a drifting drogue buoy from a ship (1). In the latter case, a high-precision navigation system is required on the ship to accurately establish the drift of the buoy. Operations with aircraft or ships are both expensive and time-consuming for the meager amount of current data obtained (one vector over a period of about 1/2 hour). The velocity accuracy of these float-locating techniques appears to be of the order of 10 to 15 centimeters per second in magnitude and 5° in angle (2). The location of such drogues by triangulation, using high-frequency (HF) surface-wave emissions from the buoy, is described in (3); although such drogues are inexpensive (\$175), the positional accuracy deteriorates with distance from shore, making this an unacceptable alternative near the edge of the continental shelf.

We discuss here a coastally located HF radar system that can measure and map near-surface currents to ranges about 70 kilometers from shore. This instrument deduces current velocity from the echoes scattered continuously from the ocean waves; buoys and drifters are not required. The radar units were built to be transportable and quickly deployable on a beach. A minicomputer controls the radar and processes the signals, permitting a current-vector map to be plotted in the field after 1/2 hour of operation. Two spatially separated radar units are presently employed, simultaneously

The authors are scientists with the Sea State Studies Area of the Wave Propagation Laboratories, Environmental Research Laboratories, National Oceanic and Atmospheric Administration, Boulder, Colorado 80302.

but independently, in order to yield the total current vector at each map grid point.

The principles underlying the system have been studied theoretically and experimentally over the past several years. The motion of the waves is seen by the radar as a translation of the frequency of the received echo signal from that of the transmitted signal; this frequency translation is called the echo Doppler shift. The radar can thus resolve and measure the component of scatter velocity along the line between the scatterer and the radar, referred to as the radial velocity. Crombie (4) first showed experimentally—and it was later confirmed theoretically (5)—that to first order the scatterers at high frequency are ocean wave trains moving toward and away from the radar, having spatial periods precisely one-half the radar wavelength. Thus the scattering mechanism is the diffraction grating or Bragg effect used in holography or in x-ray analysis of crystalline structures. The spectrum of the continuous-wave transmitted signal is a narrow peak at the carrier frequency location, as shown in Fig. 1. In the absence of current, the received first-order sea echo appears as two symmetrically spaced peaks about the carrier, whose Doppler shifts are given by the lowest-order dispersion relation of the scattering gravity waves; that is

$$\pm f_d = 2v_{ph}/\lambda = 2(gL/2\pi)^{1/2}/\lambda = (g/\pi\lambda)^{1/2} \quad (1)$$

where λ is the radar wavelength, $L = \lambda/2$ is the length of the ocean waves responsible for the first-order Bragg scattering, v_{ph} is the phase velocity of these waves, and g is the gravitational constant.

A current beneath the surface waves represents a transport of the water mass, and can be thought of as a translation of the entire coordinate frame for the waves with respect to the observer at the stationary radar on shore. Hence the two spectral peaks scattered from the waves will be shifted (with respect to the position of the carrier frequency) by a small amount proportional to the radial component of current velocity, as shown at the bottom of Fig. 1. This amount is $\Delta f = 2v_{cr}/\lambda$, where v_{cr} is the mean effective current velocity radial to the radar. In (6), radar-deduced radial current observations were compared with drifter measurements of currents at San Clemente Island; the narrow radar beam and short pulse kept the ocean patch size under observation to about 7 by 7 km. The agreement was about ± 10 cm/sec. In

these investigations (6, 7) the effect of a nonuniform current on the transport of the radar-observed surface waves was also analyzed as a function of depth.

Experiments such as those at San Clemente Island (6, 7), resolving the sea echo from narrow azimuthal sectors at high frequency, require long permanent phased-array antenna systems (> 300 m) on the beach to form a narrow beam. When one considers typical current patterns and the various echo-signal Doppler shifts they would produce at different azimuths from the radar, one can conceive of much smaller, simpler antenna systems for determining the direction of arrival of the echo. For example, by comparing the phase between two noninteracting antennas separated by less than one-half wavelength, one can uniquely determine the direction of arrival over 180° of space of a single signal at a given Doppler shift. Crombie (8) showed that this simple two-antenna system was adequate to azimuthally resolve sea-echo signals from Florida, looking eastward across the south-to-north Gulf Stream current flow.

Concepts Behind the Present System

Because seawater is nearly a perfect conductor at high frequency (3 to 30 megahertz), the "ground-wave" propagation mode is employed (9). In this mode, vertically polarized electric fields are transmitted and received. The propagating fields at these frequencies follow the curvature of the earth and continue well into the shadow region beyond the

horizon, even in the absence of atmospheric and ionospheric refractive index anomalies. Mathematical solutions for the ground wave—corrected to include the effects of sea-surface roughness (9)—are available. They show that (i) near the radiating source, the field decays with the expected inverse range dependence of free space, and (ii) far into the shadow region, the fields near the surface decay exponentially with range. This exponential range dependence ultimately dictates the maximum distance at which currents can be observed for a particular transmitted power. For the hardware described in the next section, the maximum range for the system—allowing for a 10-decibel signal-to-noise ratio (S/N) at the receiver (10)—is about 70 km; this has been verified in our recent experiments, which are discussed below.

Although the system does not employ ionospheric or atmospheric refraction to propagate beyond the horizon, it is incorrect to call it a "line-of-sight" radar (as is a microwave radar). In fact, trying to increase the useful range of the radar by elevating the antennas (in order to increase the distance to the horizon) is counterproductive, because there is a discontinuity in the propagation path in free space between the antennas and the highly conducting seawater. We have established this fact theoretically and also experimentally, by trying to put the antennas on roofs of buildings (but back several hundred meters from the water) to increase the range. We have found that the optimal locations for the antennas are at sea level on the beach, as close to the water as possible; in fact, it

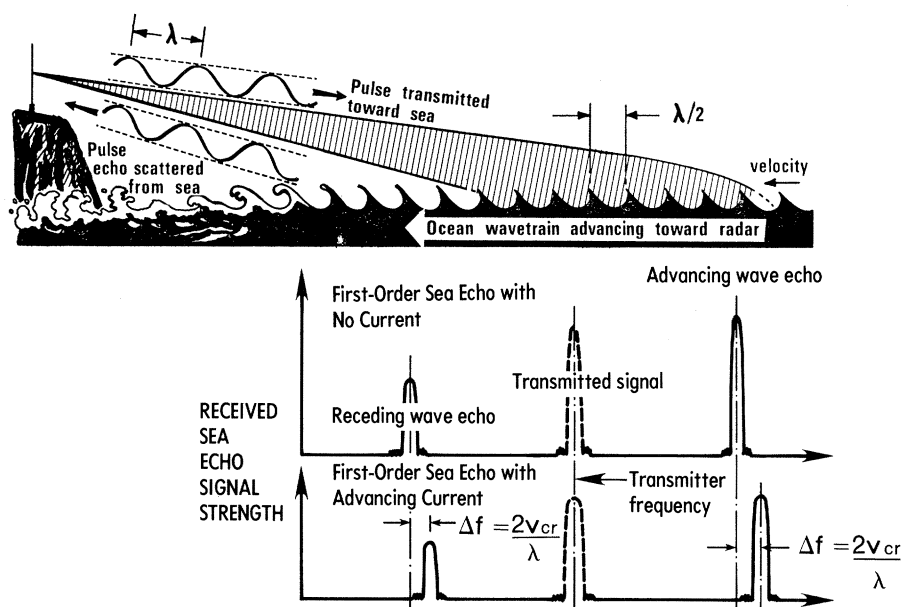


Fig. 1. Sketch showing the principles of first-order HF Bragg scatter from the sea, and resulting signal echo spectra without and with an underlying current.

is best if the grounding system beneath the antennas makes electrical contact with the seawater.

A separate antenna is used for transmitting. It produces a slightly directional pattern, peaked out toward the sea, with a half-power beam width of $\pm 90^\circ$; its radiation in the backward direction is ~ 10 db lower than that in the forward direction, which minimizes unwanted illumination over land. As with nearly all radars, time gating of the received signal echo referenced to the transmitted pulse time determines the range to the sea echo. Our system transmits a 20-microsecond unmodulated pulse and digitizes the received echo signal every 20 microseconds after transmission. The signal sample from each range (time) gate thus represents the echo from an annulus of the sea surface 3 km in width, concentric with the radar location. A total of 25 consecutive range-gated signals are thus retained for every transmitted pulse, providing a total distance of about 75 km from the radar. The transmitted pulse repetition interval is 1 millisecond.

Since echo-signal Doppler shifts are to be related to current velocities, the time series for each range gate is spectrally processed. This is done digitally at the radar site with a fast Fourier transform (FFT) algorithm. Appropriate digital filtering of the signals is performed before the FFT to prevent spectral aliasing and to maximize S/N. Since the sea surface is a random variable, the sea echo is also a random variable. In fact, each spectral power point output from the FFT is an independent random variable, following a chi-square distribution with two degrees of freedom (11).

In the first series of experiments, three colinear independent receiving antennas were employed. The received signal was sampled on each antenna separately and sequentially for each transmission every millisecond, with the other two antennas switched open to minimize mutual interactions. Therefore the FFT outputs from the three antennas (for a given range gate) can be thought of as being measured simultaneously; the only theoretical difference between the signals at the antennas is due to the phase path differences undergone by an echo, at a particular Doppler frequency from a particular direction, arriving at the different positions of the three elements. Three antenna elements, each separated for our first experiments by one-quarter wavelength (3 m at 25 Mhz), aligned parallel to a straight coastline, can unambiguously resolve two sea-echo signals at a particular Doppler frequency from 180° of space. For two signals with complex am-

plitudes \dot{A}_1 and \dot{A}_2 from angles α_1 and α_2 (with respect to the perpendicular to the coastline), the three complex received voltages \dot{V}_A , \dot{V}_B , and \dot{V}_C can be solved in closed form for the desired angles and amplitudes, with the following results (asterisks denote complex conjugates)

$$\alpha_{1,2} = \sin^{-1} \left[\frac{-\tan^{-1} \left(\frac{\text{Im}(x_{1,2})}{\text{Re}(x_{1,2})} \right)}{\pi/2} \right] \quad (2)$$

and

$$\dot{A}_{1,2} = \frac{\dot{V}_A x_{2,1} - \dot{V}_B}{(x_{2,1} - x_{1,2})} \quad (3)$$

where

$$x_{1,2} = \frac{(|\dot{V}_C|^2 - |\dot{V}_A|^2) \pm i(4|\dot{V}_C\dot{V}_B^* - \dot{V}_B\dot{V}_A^*|^2 - (|\dot{V}_C|^2 - |\dot{V}_A|^2)^2)^{1/2}}{2(\dot{V}_C^*\dot{V}_B - \dot{V}_B^*\dot{V}_A)}$$

In reality, since the sea-echo signal amplitudes \dot{A}_1 and \dot{A}_2 are random variables to which random noise is added, the angles of arrival determined from Eqs. 2 to 4 contain a random error that decreases with increasing S/N. Extensive simulations and special experiments have shown that for 10-db S/N, such angular errors are less than 1° for $|\alpha| < 70^\circ$. We have recently changed to a four-antenna configuration (arranged in a square) to resolve two signals from 360° ; this permits us to operate the radar on a peninsula or an island with ocean water subtending more than 180° around the site.

Two sites are required to obtain two radial current-vector components along lines pointing in different directions in order to construct a total current vector at a particular point on the sea. For a straight coastline, the question arises as to how far apart the sites should be. Since a total current vector can be constructed only within the common overlapping areas seen by both sites, it is desirable to maximize this area (by moving the sites closer together). On the other hand, as the sites become close (superposed in the limit), they see most points on the sea in the common area along nearly the same radial direction, which makes construction of the total vector inaccurate. Consequently, we defined the optimization criterion for site separation as the product of the common coverage area times the average of the sine of the angle between the lines to the two sites. This product has a broad maximum, indicating that for a coverage distance from a single site of about 70 km, a site spacing anywhere between 25 and 55 km is adequate.

Various trade-offs were considered in selecting the frequency range 25 to 26

Mhz for our first series of tests (the radar wavelength of 12 m is, to first order, scattered from ocean waves with a 6-m wavelength). At these frequencies atmospheric and external man-made electrical noise are often low, being equal to internal electrical receiver noise, whereas at lower frequencies atmospheric noise seen by the radar increases sharply. In addition, antenna sizes also increase with decreasing frequency, requiring larger structures and more ground area. On the other hand, ground-wave propagation loss decreases with decreasing frequency, offsetting the noise dependence. There are additional reasons for operating at higher frequencies, however. For one thing, above 25 Mhz ionospherically propagated echoes are rarely encountered, whereas at lower frequencies such distant echoes can be folded in with the desired short-range sea return. Two other important reasons for higher frequencies are oceanographic in nature. First, the Bragg-scattering 6-m ocean waves are relatively short and are likely to be present more of the time than longer waves, which require stronger winds to develop them. A wind with a velocity greater than 3 m/sec, blowing longer than 1 hour, will develop 6-m waves to their (equilibrium) root-mean-square height of ~ 10 cm. Inasmuch as the waves are used only as a "tracer" for the underlying currents, it is desirable that they be present as often as possible. Second, the shorter the ocean waves under observation, the more they are influenced by currents very near the surface. A rule of thumb (6, 7) is that the depth of the layer whose current will affect a surface wave of length L is $L/2\pi$ (about 1 m for $L = 6$ m). Hence, if one wants to observe currents in the uppermost ocean layers by measuring their effect on the phase speeds of gravity waves, he should use as high a radar frequency as possible. These factors led us to select 25 to 30 Mhz for our initial operations.

Hardware Description

The present two-unit radar system was designed as a prototype of an operational version, with considerably more flexibility than will ultimately be needed, in order to facilitate changes as experience is gained in the field. Yet this system was built to be transported by vehicle (see Fig. 2), easily erected on a beach, and capable of being operated from a portable power supply (a 2.2-kilowatt gaso-

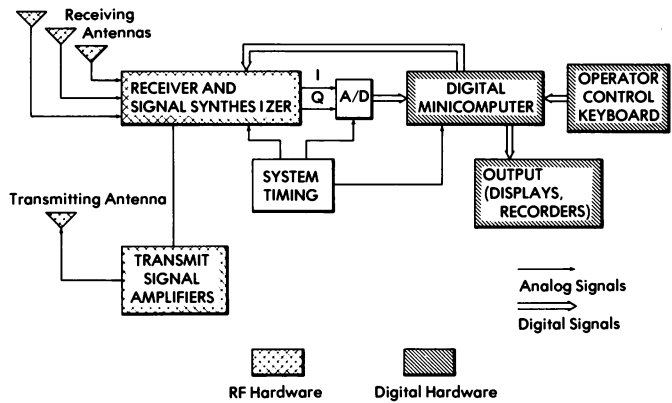


Fig. 2 (left). Sketch of the system as operated on the beach. Transmitting antennas are on the left and receiving antenna on the right. Fig. 3 (right). Block diagram of radar system.

line generator). The entire radar is controlled by a minicomputer, which also does the signal and data processing in the field. The end result is a map—drawn on a pen plotter—of the surface-current vector field.

The system radiates ~ 2.5 -kw-peak pulse power, as a stream of 20 - μ sec pulses every millisecond; thus the average radiated power is only 50 watts. The radar is presently capable of transmitting any operator-selected frequency between 25 and 35 Mhz (in 200-khz increments), but so far we have operated primarily between 25 and 26 Mhz. The transmitting antenna is a log-periodic vertical monopole array of three (or four) elements designed especially for this application at Lawrence Livermore Laboratories (12). Both versions were designed to have an input impedance of ~ 50 ohms (real) from 25 to 27 Mhz; the three-element version has a half-power beam width of $\pm 90^\circ$, while the four-element version has $\pm 43^\circ$.

The individual receiving elements are readily available fiberglass-encased citizens-band whips cut to a height of 1.575 m and each fed against a quarter-wavelength, four-element, radial ground screen. The three (and currently four) receiving elements are aligned on the beach with a tape measure and compass. These elements are each connected through one-half wavelength of coaxial cable to a switching network and preamplifier box, which cycles sequentially through each of the antennas at a rate of 1 msec per antenna. From this switch, the signals then pass through a single preamplifier and coaxial line several tens

of meters in length to the receiver hardware in the van. From the antenna switch onward, the signals from each antenna pass through the same hardware, eliminating mismatch problems through separate channels. The entire antenna system can be unfurled by two men in about 1/2 hour.

The heart of the radio-frequency system is the receiver (Fig. 3), designed by Barry Research, Inc., especially for this radar. In addition to its obvious function, the receiver also synthesizes the desired

carrier frequency and the pulse stream to be transmitted. This stream is amplified in hardware designed and built in-house. Every 20 μ sec, the receiver gain is changed under computer control, called a sensitivity time control (STC), in order to compensate for the decrease of echo strength with range. The echo is coherently mixed down to zero-intermediate-frequency in-phase and quadrature (I and Q) signals. These I and Q signals are then digitized with a ten-bit analog-to-digital (A/D) converter every 20 μ sec,



Fig. 4. Photograph of complete radar radio-frequency and digital hardware.

and all subsequent signal processing is done digitally. This includes filtering (called preaveraging, over 1/2 or 1/4 second) to reduce the signal bandwidth to 2 or 4 hertz. The filtered signals for each range gate and each receiving antenna are then collected for 128 or 256 seconds as the input to a 512-point complex FFT; thus, for the 128-second option, for example, the displayed spectrum has a Doppler resolution of 1/128 hertz over a window from -2 to $+2$ hertz. (These parameters can be selected by the operator.) The 1/128-hertz Doppler resolution translates into a radial current velocity resolution of ~ 5 cm/sec.

The heart of the digital system for radar control and data processing is a Digital Equipment Corporation PDP 11/34 minicomputer. The operator communicates with the system through a portable keyboard terminal. Moving-head magnetic disk and nine-track magnetic tape units are available for loading system software into the computer and also for recording and archiving processed radar data. Graphic displays and pen plotters are available to display raw spectra and current-vector plots. Further description of the system hardware is found in (10); a photograph of the complete digital and radio-frequency hardware (excluding antennas) for one site is shown in Fig. 4.

Experimental Results and Digital

Data Analysis

Initial field operations began with the new radar system in southern Florida during late 1976; there was an additional final week of operations in Florida from 20 to 26 March 1977, during which fairly extensive independent measurements of surface currents were made for comparisons. The Florida area was selected for initial operations and system calibrations because of the fairly regular but strong south-to-north Gulf Stream flow east of Miami. The two sites were located at South Miami Beach ($20^{\circ}46'00''N, 80^{\circ}07'58''W$) and Fort Lauderdale ($26^{\circ}05'01''N, 80^{\circ}06'38''W$), approximately 36 km apart. The latitudes and longitudes of the two sites are entered into the computer, along with the azimuthal bearings of the two receiving antenna arrays. The software then calculates the x, y positions of a rectangular grid (3 by 3 km) of points to the east of the baseline joining the two sites—at which current vectors will be plotted from the radar data—after conversion from the radar-oriented polar coordinates (range and azimuthal bearing from each site). Most of the measurements

were made on 25.4 or 25.6 Mhz, with a 128-second coherent integration time (providing a Doppler resolution of 1/128 hertz).

The output of a single FFT is a complex random variable, having Rayleigh amplitude and uniform phase probability densities. The desired first-order portion of the sea echo is random because of the statistical nature of the scattering sea surface. The remaining portion of the FFT output can be thought of as additive random noise with respect to its effect on the desired first-order signal. In reality, there are at least four types of noise, originating from different sources: (i) external atmospheric or man-made noise, (ii) internal receiver noise, (iii) second-order radar sea echo (13), and (iv) processor noise due to limited system dynamic range, system nonlinearities, and quantization noise. Finally, the actual current field beneath the waves, instead of being uniform, is more likely to be somewhat turbulent within the spatial resolution scales seen by the radar. Hence, the total signal plus noise is ran-

dom, and from this we intend to extract (i) an estimate of the azimuth angle of arrival of the signal at each Doppler frequency output from the FFT, (ii) an estimate of the radial current velocity at this range and azimuth, and (iii) the sea-echo signal amplitude.

Since extraction of the angle of arrival, using the equations given above, requires the use of coherent simultaneous signals from each of three (or four) receiving antennas for a given range cell, we cannot average the individual outputs of the FFT's in order to reduce the effects of random signal fluctuation and noise. Instead, we go through the following process. Figure 5 is an example of the right half of the amplitude-squared output of the FFT processor for the 37.5-km range gate for sea echo measured at Fort Lauderdale. A threshold level is established for the usable portion of the signal (for example, 20 db down from the mean peak level), and the remainder of the FFT output is discarded. The solid curve shows the expected position of the echo in the absence of any current over the semicircular range cell; it occurs at a Doppler shift f_d (Eq. 1). All echo points at Doppler shifts different from f_d are therefore due to currents, and a radial current velocity scale centered on f_d can be given in terms of these Doppler shifts, as shown in Fig. 5. The angle of arrival of the signal at each of these Doppler shifts (or radial current velocities) is then obtained from the complex signals $\hat{V}_A, \hat{V}_B,$ and \hat{V}_C at each of the three antennas, using Eqs. 2 to 4.

At this point, for a given 128-second run and for each range gate, we have an array of azimuth angles and signal echo amplitudes as a function of radial current velocity. We then interchange the roles of the dependent and independent variables, considering radial velocity as a function of azimuth angle. After accumulating and storing radial velocity data over several consecutive 128-second runs (typically ten), we then average the radial velocities that fall within preset angular "bins."

This averaging is actually done in a manner that gives preference to higher-quality points. First of all, each sample radial velocity point in a particular angular bin is weighted by the ratio of the signal (amplitude squared) to the average noise power level for that same point; higher signal amplitude values give more accurate angle estimates. Second, other quality factors are used to weight the radial velocity samples. For example, in the absence of noise, the amplitudes of $x_{1,2}$ given in Eq. 4 will always be unity. Hence samples whose values of $|x_{1,2}|$ de-

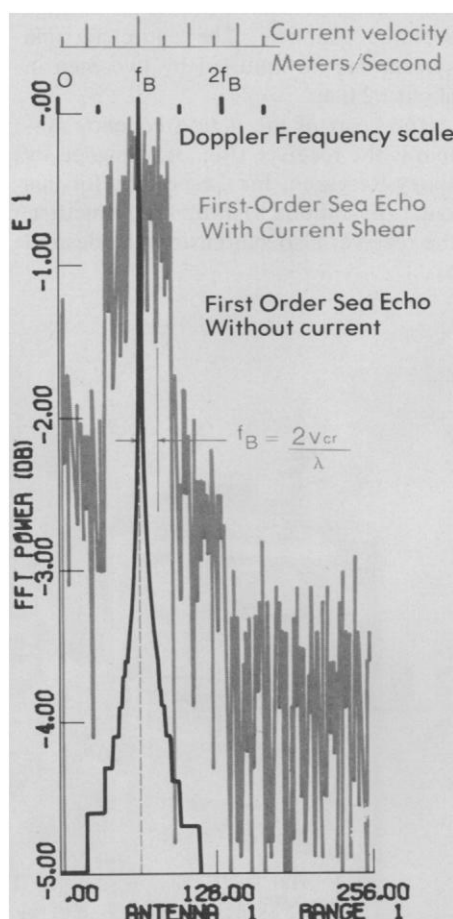


Fig. 5. Plot of FFT spectral power output. The black spectrum is the idealized test sea-echo spectrum in the absence of a current. The gray spectrum is the measured sea echo at 37.5 km from Fort Lauderdale, as modified by Gulf Stream current shear.

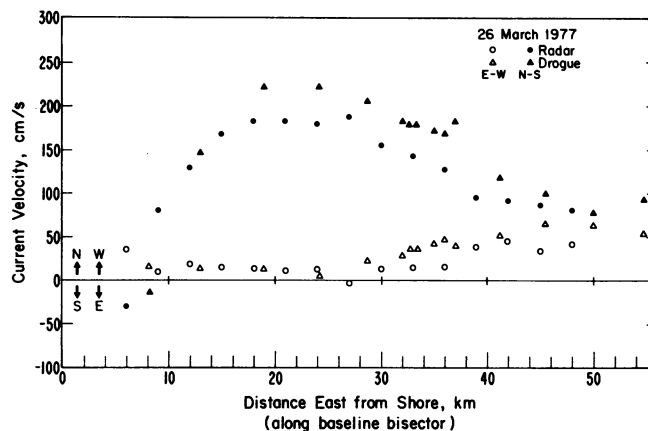
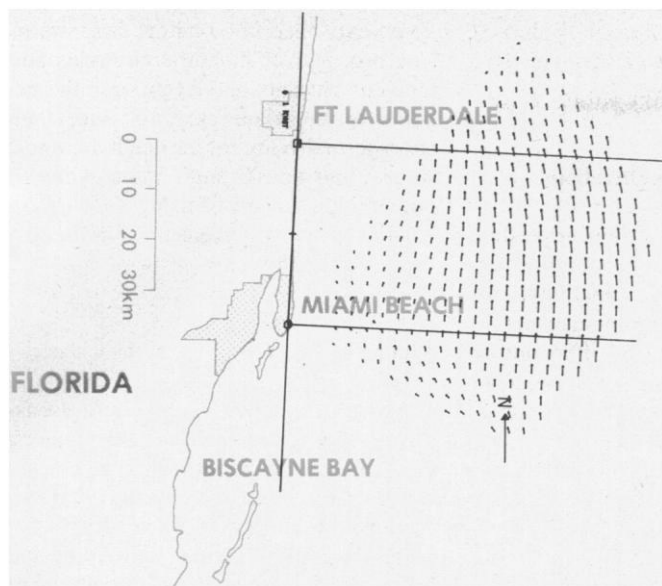


Fig. 6 (left). Computer-generated map of the Gulf Stream current on 20 October 1976 as deduced by radar. Fig. 7 (right). Comparison of radar-deduced surface currents and drifter measurements, resolved into north-south (solid symbols) and east-west (open symbols) components.

part significantly from unity are weighted lower. Finally, the signal-to-noise ratios for all of the samples in a particular angular bin are averaged; this is used in a final thresholding process to decide whether the (weighted) averaged radial velocity for that bin will ultimately be used. If it is not used (because the signals are too low) or if there were no values falling in the bin, then a value for the radial velocity at that angle is calculated by interpolation from the adjacent range-azimuth cells.

In the process of producing a map, the data from both sites are combined (in our case, either by data telemetry between the two sites or by physically transporting the data tapes from one site to the other). Then the arrays of radial current velocities from each radar site together with range and azimuth (in polar coordinates) are entered for each rectangular grid point; also, direction cosines at the grid point are calculated for the radial lines to the sites. This allows the total current vector to be plotted at that grid point. The angular sectors very near the shore are sometimes excluded because the nearly parallel radial velocities seen from each site at these grid points give rise to large vector errors; integration techniques to improve the quality of the maps near shore are being investigated. Figure 6 is an example of a map made in Florida by using these data processing steps. The well-known horizontal shear of the Gulf Stream (outward from the shore) is clearly visible in these maps.

The point to be emphasized is that all of the averaging, weighting, and thresholding procedures described above are done digitally (not arbitrarily or subjectively), according to rules that are being

optimized. The mathematical steps involved, beginning with the angle extraction, are nonlinear in nature. Hence it is not possible to obtain mathematical error estimates in closed form. The optimization of the processing algorithms must therefore be based on two methods of quality assessment. First, simulations are employed in which one begins with known current patterns, randomizes the first-order sea-echo spectrum, adds random noise, converts to a time series, and then processes this simulated echo signal to see how well the original current patterns are recovered. We have been using such simulations for nearly 3 years to arrive at our present algorithms. Second, independent measurements of surface currents are obtained during radar operations, using drifters and timed-released floats. Comparisons of these measurements with radar data are the subject of the next section.

Comparison with Drifters

As an ultimate calibration standard, one would like to employ independent measurements of near-surface currents as "ground truth." However, since differences of tens of centimeters per second have been documented in drifter current measurements, there is considerable doubt as to whether disagreements of this order between drifter and radar-deduced currents are due to radar errors or drifter errors. Furthermore, the two techniques are so dissimilar in nature that there are many reasons why they should respond differently to conditions near the surface. Nonetheless, since drifters are the only established quantitative method of esti-

mating surface currents, we made a series of radar measurements on 23 to 26 March 1977 in Florida in conjunction with ship tracks of drifters in order to establish some initial credibility for this new remote-sensing technique. The Nova University vessel *Youngster III*—supported by a Hi-Fix Navigation system—tracked a drifter at several positions in the radar coverage area over 8- to 12-hour periods on 23 and 25 March. This drifter was drogued with rigid vertical aluminum baffle plates extending 46 cm below the surface float. Each track consisted of a 5- to 8-minute drift whose start and end points were marked navigationally; from this a mean (Lagrangian) drift velocity was calculated. In addition, the National Oceanic and Atmospheric Administration vessel *Virginia Key*—supported by a miniranger navigation system—tracked a cork float on 23 and 24 March at other locations in the coverage area. Again, each track lasted about 5 minutes.

The velocities deduced from both radar and drifter measurements, and the differences between them, were relatively similar in all cases. Significantly, the drifter velocities show considerable differences from day to day. For comparison, we show here our longest set of drifter measurements, made eastward from shore (at the midpoint between the two radar sites) to a range of 50 km; these drifter measurements, made with the *Youngster III* and the drogued buoy, required 12 hours to complete. These measurements are shown in Fig. 7 along with radar-deduced current velocities. The north-south and east-west components of the total velocity vectors are plotted in each case.

The agreement is very reasonable,

within the range of the expected drifter variances. Of possibly greater significance than the actual differences are the facts that (i) both the radar and the drifter observed the "countercurrent" flowing toward the south close to shore (this current element is seen only occasionally, and was not observed with the radar or drifters on the other 2 days); and (ii) both instruments recorded the considerable current shear with distance from shore. This shear was also seen to be variable in its magnitude and position from day to day. The maximum difference between the currents determined by the two techniques is about 50 cm/sec. The root-mean-square difference from this plot is 27 cm/sec, defined as

$$\left[\frac{1}{L} \int_0^L d^2(x) dx \right]^{1/2}$$

where d is the difference between straight-line segments joining radar and buoy points and L is the total length of the common path over which the two sets of measurements were made.

There are many possible explanations for the differences between the two techniques. First the radar was observing a wave phase-velocity change due to currents in a (mean) layer 1m thick, while the drogue felt currents only within the top 0.46-m layer. Since currents nearest the surface are known to differ most from deeper currents, this may explain some of the difference. Second, some of the buoy motion was directly due to the wind; during the ship measurements over the easternmost 20 km, a strong wind (~12 m/sec) blew from the east-southeast. Third, breaking waves, which were prevalent with the high wind and wave conditions on these days, entrain floating surface objects, pushing them along (over short distances) at a much greater wave phase velocity. Fourth, the drifter and radar measurements at some locations were of necessity made several hours apart. And fifth, the drifter measurement is Lagrangian in nature, aver-

aged only over a short line (400 to 1000 m); the radar measurement is Eulerian, averaged over an area of about 3 by 3 km.

Applications and Future Directions

The HF radar remote-sensing system appears to provide considerably expanded observational capability for coastal physical oceanographic research. Since it is transportable and offers output current maps on site in near real time, the system has a great potential for operational coastal current monitoring and for quick response to offshore accidents. Inasmuch as surface currents are highly variable, elusive, and expensive to measure by existing in situ techniques, this instrument offers an attractive alternative. To duplicate the large areal volume of data vectors obtained with only a 1/2-hour radar operation would require many ships or aircraft tracking drifters simultaneously—an experiment that would cost hundreds of thousands of dollars. Our discussion with commercial manufacturers lead us to believe that streamlined operational versions of our prototype radar could be available for about \$50,000 per complete radar pair.

The need to understand and better define the structure of currentlike water movement near the surface becomes more evident as we attempt to further interpret and refine the accuracy of this system. Both theoretical analyses and carefully planned experiments should be undertaken to quantify the effects of current turbulence within the radar cell, wave-wave interactions, and current shear with depth on the radar measurements. Furthermore, the actual linear horizontal drift of particles at the surface (for example, oil) and its relation to mean near-surface current velocity must be determined, especially under conditions of high winds and breaking waves. The similarities and differences between Eule-

rian areal and Lagrangian linear measurements need to be better understood. The prospect of having continuous surface-current data should provide the impetus to correlate currents with their short-term driving forces (such as winds, waves, and tides). Such a correlation is potentially a means of using the surface-current data to measure, indirectly, those driving forces.

Summary

A high-frequency radar remote-sensing system for measuring and mapping near-surface ocean currents in coastal waters has been analyzed and described. A transportable prototype version of the system was designed, constructed, and tested. With two units operating tens of kilometers apart, the currents were mapped in near real time at a grid of points 3 by 3 km covering areas exceeding 2000 km², out to a distance of about 70 km from the shore. Preliminary estimates of the precision of current velocity measurements show it to be better than 30 cm/sec.

References

1. P. M. Saunders, *Deep-Sea Res.* **23**, 249 (1976).
2. V. Klemas, G. Davis, J. Lackie, W. Whelan, G. Tornatore, *IEEE Trans. Geosci. Electron* **GE-15**, 97 (1977).
3. W. S. Richardson, H. J. White, Jr., L. Nemeth, *J. Mar. Res.* **30**, 259 (1972).
4. D. D. Crombie, *Nature (London)* **175**, 681 (1955).
5. D. E. Barrick, *IEEE Trans. Antennas Propag.* **AP-20**, 2 (1972).
6. R. H. Stewart and J. W. Joy, *Deep-Sea Res.* **21**, 1039 (1974).
7. D. E. Barrick, J. M. Headrick, R. W. Bogle, D. D. Crombie, *Proc. IEEE* **62**, 673 (1974).
8. D. D. Crombie, in *Proceedings of the IEEE Ocean '72 Conference* (IEEE Publ. 72 CHO 660-1 OCC, Institute of Electrical and Electronics Engineers, New York, 1972), pp. 173-179.
9. D. E. Barrick, *Radio Sci.* **6**, 517 (1971).
10. _____ and M. W. Evans, *NOAA (Natl. Oceanic Atmos. Adm.) Tech. Rep. ERL 373-WPL 47* (1976).
11. D. E. Barrick and J. B. Snider, *IEEE Trans. Antennas Propag.* **AP-25**, 19 (1977).
12. J. L. Willows and R. J. Lytle, *Lawrence Livermore Lab. Rep. UCID-17024* (1976).
13. D. E. Barrick, in *Remote Sensing of the Troposphere*, V. E. Derr, Ed. (Government Printing Office, Washington, D.C., 1972), chap. 12.